Sakarya University Journal of Science
SAUJS

Title: Numerical Investigation of The Effect of Impeller Blade Angle for Stirred Tank

Authors: Dogan Engin ALNAK, Ferhat KOCA, Yeliz ALNAK

Numerical Investigation of The Effect of Impeller Blade Angle for Stirred Tank

Dogan Engin ALNAK*[1], Ferhat KOCA[1], Yeliz ALNAK[1]

Abstract

In this study, the most widely used Rushton turbine in the industry was discussed, and the effect of different blade angles on the mixture was investigated numerically. As a standard model, 6 bladed propellers were used and 4 baffles were placed in the stirred tank. The selected tank model is in the form of a flat bottom cylindrical container. Flow characteristics were obtained by giving angles (10°, 20°, 30°, 40°, 50°, 60°) to the propeller blades used in the straight model. The obtained results were compared with each other. In addition, analyzes were repeated at different rotation speeds (600 rpm, 750 rpm, 1000 rpm) for each model at each angle. ANSYS Fluent 18 commercial software, which is the most preferred CFD program in the literature, was used for this numerical study. The analyzes were provided in the standard k-epsilon (ε) turbulence model. The Multiple Reference Frame (MRF) approach was used to simulate impeller rotation. The velocity profiles obtained from the simulations have been shown to be in consistent with the experimental estimates and the results of previous studies. As a result, it has been revealed that the best mixing balance is provided by the impeller blade at 40 and 50 degrees.

Keywords: Stirred tank, agitator, propeller design, computational fluid mechanics, k-epsilon turbulence model.

1. INTRODUCTION

Mixing is the creation of two or more materials physically or chemically or both ways in order to increase the homogeneity of the mixture. The main purpose of mixing is to increase homogeneity. The devices performing this process are called agitator or mixer (stirred tank). The physical properties and mixing ratios of the materials are one of the most important factors affecting the mixing process. Since the existence of human beings, mixing processes have been continuously investigated and a standard has been tried to be established for the mixtures created. Stirred tanks consist of several pieces of equipment. These parts are a mixer, tank and power mechanism. Depending on the properties of the mixed materials, these tanks may require additional equipment. From past to present, stirred tanks have been diversified according to the physical conditions of the materials (solid, liquid, gas) and the difficulties encountered

* Corresponding author: dealnak@cumhuriyet.edu.tr
[1] Sivas Cumhuriyet University, Faculty of Technology, Department of Manufacturing Engineering, Department of Energy Systems
E-mail: ferhatkoca@cumhuriyet.edu.tr, ytas@cumhuriyet.edu.tr
ORCID: https://orcid.org/0000-0003-0126-1483, https://orcid.org/0000-0001-8849-5295, https://orcid.org/0000-0003-4383-3806

during use have been minimized. Therefore, stirred tanks attract the attention of researchers [1-9]. Naeeni and Pakzad simulated the mixture of liquid-liquid dispersion in their study. They simulated the mixing of water with crude oil by CFD in a tank using a standard Rushton Turbine. Four different types of crude oil and tap water were used in their study. They confirmed that the viscosity increases with the increase of the impeller speed, and the homogeneity increases with the decrease in the size of the droplets [10]. Farhad et al. investigated the effects of impeller type on mixing of high concentration mixtures. They used 3 different propeller types in the study; standard A310 propeller, PF3 propeller and 4 blade propeller. They showed that the most efficient propeller among them is the propeller with 4 blades. They emphasized that the mixture is more homogeneous, more efficient at the same power consumption and more effective in suspending solid particles [11]. Ameur et al. studied the flow patterns of the differences between radial impellers and a Rushton turbine in a cylindrical mixing tank of a viscous Newtonian liquid. They reported that the radial propeller was inefficient at low Re value, the jet became stronger with increasing Re value and thus improved axial circulation was provided. In the fully turbulent regime the radial impeller showed a stronger radial jet flow than the Rushton turbine. They also showed that the Rushton turbine provides a stronger tangential flow compared to the other radial propeller and that it is more efficient and increases the area with increased homogeneity [12]. Gu et al. made a numerical simulation of the new propeller designed by placing a rigid object with a hole between two propellers. In addition, they made comparisons with the models they placed without a rigid body in between and a rigid body without a hole. Of these new propellers designed by researching on various qualities, the one with a perforated rigid body was found to be more efficient, while the one without a hole was found to be more efficient than the system with two propellers [13]. González-Neria et al. compared the PIV and dynamic LES analysis of turbulent flow in a mixing tank mixed by a four-blade propeller with a v-groove. According to the results of the study, the v-grooved propeller showed a higher

performance and provided a faster mixing [14]. Wadnerkar et al. conducted and investigated CFD simulation of solid liquid mixing tanks in low to dense solid loading systems. They used cylindrical, flat-bottomed tank with baffles and a six-bladed Rushton turbine. They performed simulations using the euler-euler multiphase model. They stated that there is maximum turbulence kinetic energy in the propeller region. They also stated that as the concentration of the solid increases, the turbulence disappears [15]. Qi et al. conducted a CFD simulation of the particle suspension in the stirred tank. They modeled a tank with baffles using a Smith türbine. k-ε and eulerian-eulerian turbulence model was employed. They saw a region where solid and liquid had low velocity due to the accumulation of solid particles at the bottom of the tank. They said that the effect of higher density and smaller diameter particles on suspension homogeneity is minimized when the particles are placed in a more viscous liquid [16]. Alcamo et al. modeled the turbulent flow in a tank without baffles using LES with Smagorinsky model. They used the standard Rushton turbine as the propeller and ANSYS-CFX 4.4 as the software. They showed that there was a pair of rear vortices known to exist in tanks with baffles and verified in tanks without baffles. They compared the results with the experimental data and showed that they were in consistent [17].

In this study, Rushton turbine stirred tank model with flat bottom, 4 baffles and standard 6 blades was considered. The main research topic is how Rushton turbine blade structure affects the mixing structure when it is inclined 10°, 20°, 30°, 40°, 50°, 60°. In addition, the effect of different angular speeds (600 rpm, 750 rpm and 1000 rpm) on flow characteristics was investigated for each inclined blade structure. ANSYS Fluent 18 commercial software, which is the most preferred CFD program in the literature, was used for the numerical study. The analyzes were provided in the standard k-epsilon (ε) turbulence model. The Multiple Reference Frame (MRF) approach is used to simulate impeller rotation.

2. NUMERICAL WORK AND MATHEMATICAL FORMULAS

The stirred tank configuration used for simulation in this study is same as Torotwa and Ji [18] as shown in Figure 1. The shaft holding the impellers had a diameter of 0.012 m and were positioned concentric to the axis of the tank. Baffles were included in the set-up to prevent the liquid from spinning as a single body. The outline of the experimental tank and the dimensions of the agitation components are shown in Figure 1 and Table 1 respectively.
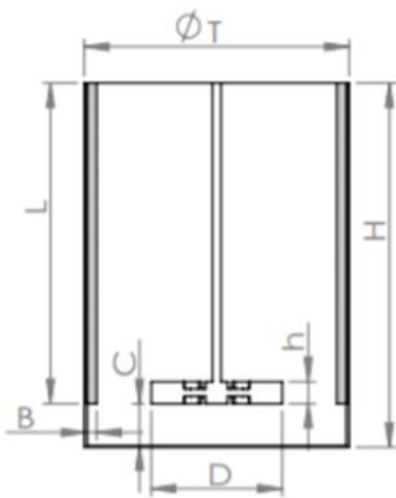

Figure 1 Diagram of the numerical set-up

Table 1 Dimensions of the strirred tank

Parameter	Symbol	Value (mm)
Tank diameter	T	360
Tank height	H	500
Impeller diameter	D=T/2	180
Impeller blade height	H	10
Baffle length	L	440
Baffle width	B=D/12	15
Impeller clearance	C=D/3	60

The Multiple Reference Frame (MRF) motion technique was used to simulation of impeller rotation. In this method, the flow in the impeller region is solved in a rotating framework while the outer region is solved in a stationary reference frame. The boundary of the inner rotating region was positioned from C = 60 mm (where C is the axial distance from the bottom of the vessel) with D = 180 mm. The Enhanced Wall Treatment function was chosen to enhance the solution by giving advantage for selected RPM (600, 750, 1000) and fine meshes. The simulation was performed using CFD software Ansys Fluent 18 solver where a control-volume-based technique was used to convert the general scalar transport equations to algebraic equations and then solved numerically using the pressure-based solver with segregated algorithm. Simulations were performed using the "COUPLED" scheme to model the Pressure-Velocity coupling, the "PRESTO! (Pressure Staggering Option)" to model the pressure and the "Second Order Upwind" scheme for the momentum, turbulent kinetic energy and turbulent dissipation rate. A maximum convergence criterion of 10-6 was set for the simulation and the case was conducted steady. The total simulation time for each case was around 30 h and residual target of 10-4 was reached within 5000 iterations. Flow behavior inside stirred tank is solved by discretized governing equations. The governing equations are the Navier–Stokes equations, which solve the mass and momentum conservation equations and provide solution for flow variables such as velocity and pressure. The continuity or mass conservation equation is given by

Continuity equation

$$\frac{\partial \bar{u}}{\partial x} + \frac{\partial \bar{v}}{\partial y} + \frac{\partial \bar{w}}{\partial z} = 0 \tag{1}$$

Momentum equation

x direction momentum equation

$$\left[\bar{u}\frac{\partial \bar{u}}{\partial x} + \frac{\partial \overline{(u')^2}}{\partial x}\right] + \left[\bar{v}\frac{\partial \bar{u}}{\partial y} + \frac{\partial \overline{(u'v')}}{\partial y}\right] + \left[\bar{w}\frac{\partial \bar{u}}{\partial z} + \frac{\partial \overline{u'w'}}{\partial z}\right] = -\frac{1}{\rho}\frac{\partial \bar{p}}{\partial x} + v\left(\frac{\partial^2 \bar{u}}{\partial x^2} + \frac{\partial^2 \bar{u}}{\partial y^2} + \frac{\partial^2 \bar{u}}{\partial z^2}\right) \tag{2}$$

y direction momentum equation

$$\left[\bar{u}\frac{\partial \bar{v}}{\partial x} + \frac{\partial \overline{(v')^2}}{\partial x}\right] + \left[\bar{v}\frac{\partial \bar{v}}{\partial y} + \frac{\partial \overline{(v'v')}}{\partial y}\right] + \left[\bar{w}\frac{\partial \bar{v}}{\partial z} + \frac{\partial \overline{v'w'}}{\partial z}\right] = -\frac{1}{\rho}\frac{\partial \bar{p}}{\partial y} + v\left(\frac{\partial^2 \bar{v}}{\partial x^2} + \frac{\partial^2 \bar{v}}{\partial y^2} + \frac{\partial^2 \bar{v}}{\partial z^2}\right) \tag{3}$$

z direction momentum equation

$$\left[\bar{u}\frac{\partial \bar{w}}{\partial x} + \frac{\partial \overline{(w')^2}}{\partial x}\right] + \left[\bar{v}\frac{\partial \bar{w}}{\partial y} + \frac{\partial \overline{(w'v')}}{\partial y}\right] + \left[\bar{w}\frac{\partial \bar{w}}{\partial z} + \frac{\partial \overline{w'w'}}{\partial z}\right] = -\frac{1}{\rho}\frac{\partial \bar{p}}{\partial z} + \nu\left(\frac{\partial^2 \bar{w}}{\partial x^2} + \frac{\partial^2 \bar{w}}{\partial y^2} + \frac{\partial^2 \bar{w}}{\partial z^2}\right) \quad (4)$$

Simulation was employed using realizable Reynolds-Averaged Navier-Stokes (RANS) k–ε model for single-phase. The reason for applying the RANS-based solution model is its advantageous use in terms of computer hardware, human effort and computation time compared to DNS or LES models. The fluid in the tank was assumed to be homogeneous and incompressible, and that the various components of the fluid had the same velocity distribution, pressure and flow pattern. The realizable k-ε model was used to specify the characteristics of turbulence and determine the basis of flow phenomena by the following equations.

The steady flow turbulance kinetic energy equation

$$\frac{\partial(\rho u k')}{\partial x} + \frac{\partial(\rho v k')}{\partial y} + \frac{\partial(\rho w k')}{\partial z} = \frac{\partial}{\partial x}\left(\frac{\mu_t}{\sigma_k}\frac{\partial k'}{\partial x}\right) + \frac{\partial}{\partial y}\left(\frac{\mu_t}{\sigma_k}\frac{\partial k'}{\partial y}\right) + \frac{\partial}{\partial z}\left(\frac{\mu_t}{\sigma_k}\frac{\partial k'}{\partial z}\right) + \mu_t\phi - \rho\varepsilon \quad (5)$$

Turbulance viscosity

$$\mu_t = C_{\mu'}\rho\frac{k'^2}{\varepsilon} \quad (6)$$

the k-ε turbulance model used in the present study, ε indicates turbulance distribution while k' and ϕ show turbulance kinetic energy and viscous dissipation term, respectively.

Turbulance kinetic energy

$$k' = \frac{1}{2}\left(\overline{u'^2} + \overline{v'^2} + \overline{w'^2}\right) \quad (7)$$

Viscous dissipation term

$$\phi = 2\mu\left[\left(\frac{\partial u}{\partial x}\right)^2 + \left(\frac{\partial v}{\partial y}\right)^2\right] + \mu\left(\frac{\partial v}{\partial x} + \frac{\partial u}{\partial y}\right)^2 \quad (8)$$

Turbulence kinetic energy disappearance equation

$$\frac{\partial(\rho u\varepsilon)}{\partial x} + \frac{\partial(\rho v\varepsilon)}{\partial y} + \frac{\partial(\rho w\varepsilon)}{\partial z} = \frac{\partial}{\partial x}\left(\frac{\mu_t}{\sigma_\varepsilon}\frac{\partial \varepsilon}{\partial x}\right) + \frac{\partial}{\partial y}\left(\frac{\mu_t}{\sigma_\varepsilon}\frac{\partial \varepsilon}{\partial y}\right) + \frac{\partial}{\partial z}\left(\frac{\mu_t}{\sigma_\varepsilon}\frac{\partial \varepsilon}{\partial z}\right) + C_{1\varepsilon}\mu_t\frac{\varepsilon}{k'}\phi - C_{2\varepsilon}\rho\frac{\varepsilon^2}{k'} \quad (9)$$

C_μ, $C_{1\varepsilon}$, $C_{2\varepsilon}$, σ_k and σ_ε that are model constants are typical default values used in the standard k-ε turbulence model [19]. The values of these constants have provided by numerous data fitting iterations for many turbulent flows.

3. MODELS

In the study, numerical studies were carried out using the Rushton turbine model. 6 propeller blades were used in the main model, which was determined as straight model, and 4 baffles were placed in the stirred tank. The selected tank model is in the form of a flat bottom cylindrical container. The results were obtained by giving angles (10°, 20°, 30°, 40°, 50°, 60°) to the propeller blades used in the flat model. The obtained results were compared with each other. These results at different rotation speeds (600 rpm, 750 rpm, 1000 rpm) were repeated for the model at each angle created. Models are shown in Figure 2.

straight propeller blade

10° inclined propeller blade

20° inclined propeller blade

30° inclined propeller blade

40° inclined propeller blade

50° inclined propeller blade
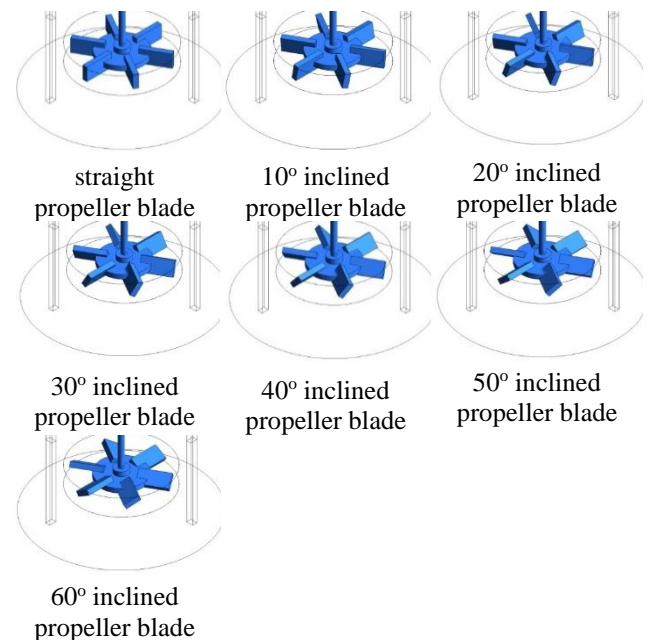
60° inclined propeller blade

Figure 2 View of the propeller models used in the study

4. MESH STRUCTURE

Hybrid mesh structure is used in the study. The total mesh number of the model was chosen as 922973 pieces. 4 different mesh numbers counted for mesh independence were determined as reference. Evaluated mesh numbers and evaluation parameter (pressure) variation are given in Table 2.In the comparison of these reference mesh numbers, when the selected mesh number was exceeded, no change was observed in the results.

Tablo 2 Pressure variation according to the number of mesh elements

Element Nu.	510363	751655	922973	1205030
P (Pa)	7850	7920	8000	8010

The mesh structure of the model is shown in Figure 3. A 20-layer mesh structure was applied on the wing surfaces, baffle surfaces and tank interior surfaces, where the fluid's non-slip condition occurs and where the most interaction occurs, and a finer mesh is formed in the areas close to these surfaces. The applied mesh structures were analyzed in the same and approximate number of elements in all models.
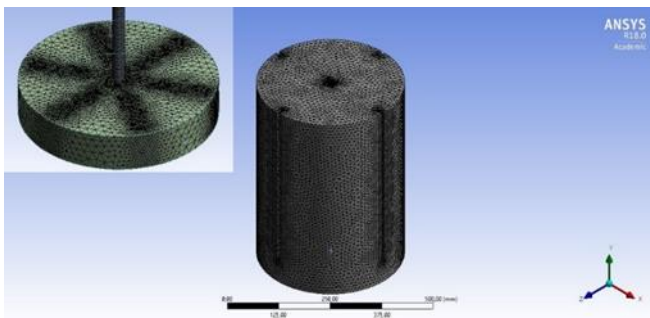

Figure 3 Structural view of mesh structure

Before the mixing simulations, it is also necessary to confirm the validity of the CFD model used in this work for stirred tank systems. The predicted results were verified by the numerical data of Duan et al. As seen from Figure 4, the predicted radial and axial profiles of azimuthally-averaged velocity components of the liquid is close to the numerical data of Duan et al. [20] respectively. The present study curve shown with the dotted line is in consistent with the work of Duan et al. shown straight line.
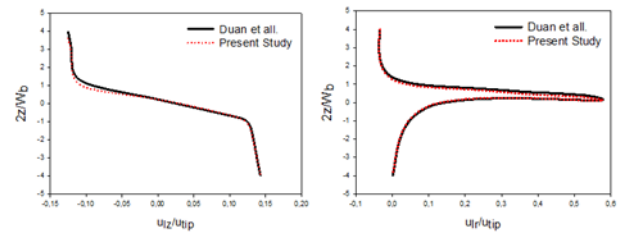

Figure 4 Comparison numerical datas with the study of Duan et al. [20]

5. RESULT

Numerical results were obtained at 600 rpm, 750 rpm and 1000 rpm turbine rotation speeds for different blade angles. Turbulence kinetic energy distributions and velocity vectors obtained for the propellers rotated at 600 rpm are given in Figure 5 for straight blade, 10° inclined blade, 20° inclined blade, 30° inclined blade, 40° inclined blade, 50° inclined blade and 60° inclined blade, respectively.

When these figures are examined, it is seen that the turbulence kinetic energy values are high at the blade tips. The formation of turbulence and flow eddies behind the blades causes the flow not to occur in those regions or to occur partially. Therefore, in these regions where the flow decreases, the decrease in inertia forces and the coincidence of the reverse flow reflected from the wall due to the effect of the baffles increased the turbulent kinetic energy. In addition, it is clearly seen in these figures that the turbulent kinetic energy is higher in the regions close to the propeller blades. Also in this rotation speed (600 rpm), although the highest instantaneous changes of turbulence kinetic energies are observed in straight blade compared to other structures, it can be observed the highest value at the models with inclination of 40° and 50° throughout the tank. In general, it is seen that the impeller with the lowest turbulence kinetic energy throughout the tank are 10° and 60° inclined blades. When the figures are examined, it is obvious that there are regions where the flow of change consisting of velocity vectors accelerates, the vicinity of the blades and the regions close to the tank walls. The reason for this event is the increase in the pressure applied to the blade with the swirling movements on the flow created by the blades, and also the points where the opposite flows hitting the tank walls

intersect with the flows from the blade. It is observed that the velocity vectors make eddies around the blades. The reason for this is the swirling movements created by the blades on the flow, and the points where the opposite flows which hit the tank walls, intersect with the flows from the blade, with the increase of the pressure applied to the blade.

straight propeller blade (TKE) — straight propeller blade (velocity vectors)

10º inclined propeller blade (TKE) — 10º inclined propeller blade (velocity vectors)

20º inclined propeller blade (TKE) — 20º inclined propeller blade (velocity vectors)

30º inclined propeller blade (TKE) — 30º inclined propeller blade (velocity vectors)

40º inclined propeller blade (TKE) — 40º inclined propeller blade (velocity vectors)

50º inclined propeller blade (TKE) — 50º inclined propeller blade (velocity vectors)

60º inclined propeller blade (TKE) — 60º inclined propeller blade (velocity vectors)
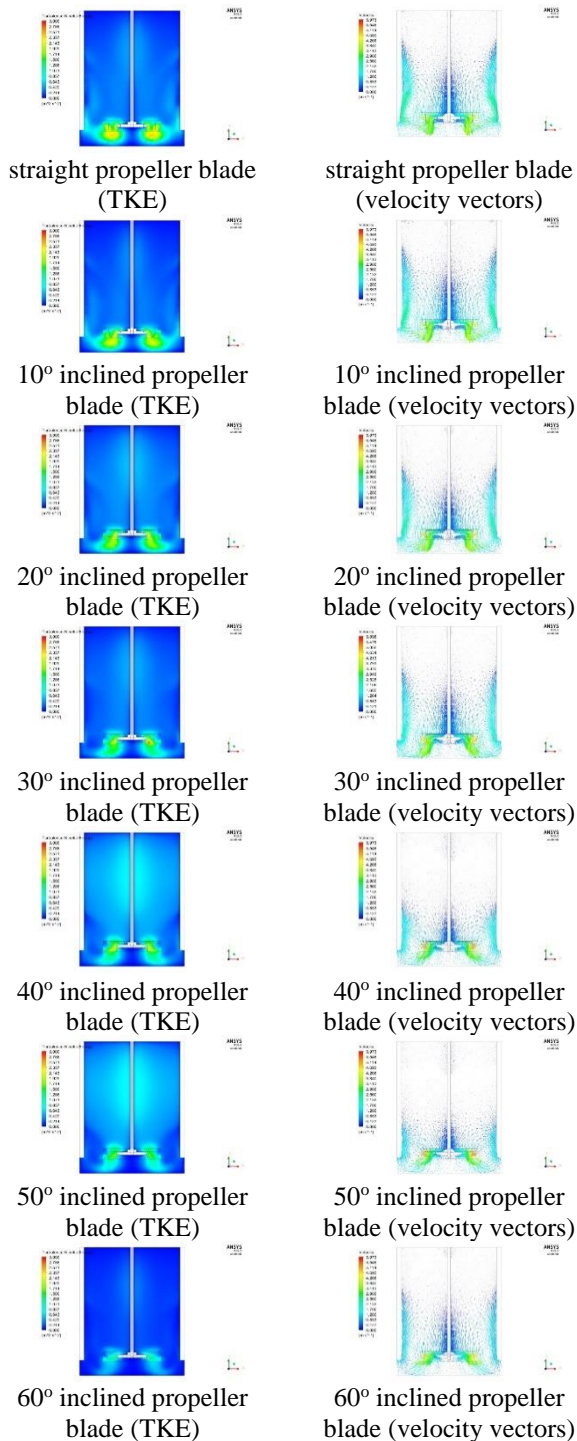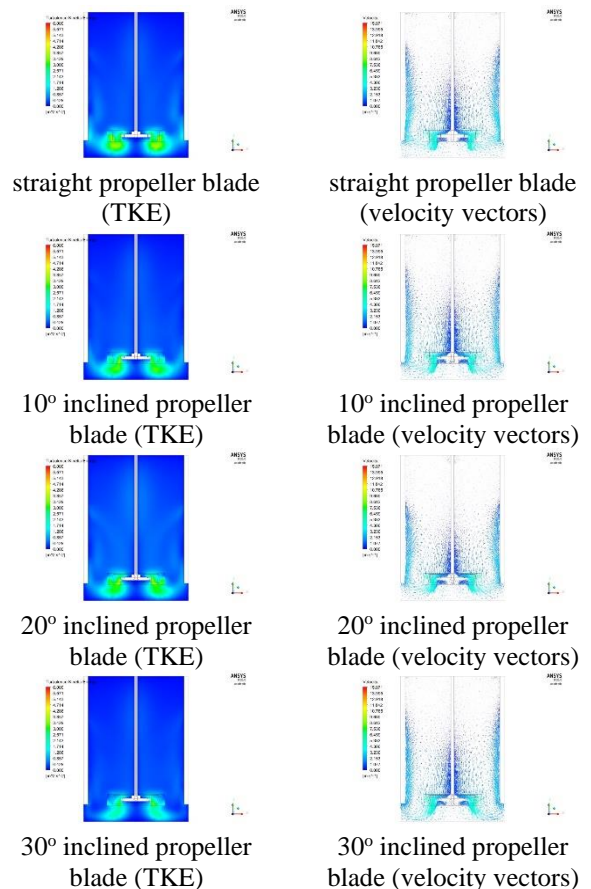
Figure 5 Model blades at 600 rpm (a) turbulence kinetic energy distribution (b) velocity vectors

Turbulence kinetic energy distributions and velocity vectors obtained for the propellers rotated at 750 rpm are given in Figure 6 for straight blade, 10° inclined blade, 20° inclined blade, 30° inclined blade, 40° inclined blade, 50° inclined blade and 60° inclined blade, respectively. When these figures are examined, it is seen that turbulence kinetic energy values are high at the blade tips, as in the visuals examined at 600 rpm. Vortex movements around the wing can be seen from the results where turbulent kinetic energy and velocities are high. It is observed that the flow changes direction due to the vortex movements in the regions between the blade and the tank bottom. According to the data obtained, it is seen that the maximum turbulence kinetic energy at 600 rpm increased from 3000 m2/s2 to 6000 m2/s2 at 750 rpm. Likewise, looking at the velocity vectors, it was observed that the maximum speed increased from 5,973 m/s to 15,071 m/s. It can be said that, with the increase in speed, the mixture achieves better results and therefore the mixture becomes more homogeneous compared to the mixes at 600 rpm.

straight propeller blade (TKE) — straight propeller blade (velocity vectors)

10º inclined propeller blade (TKE) — 10º inclined propeller blade (velocity vectors)

20º inclined propeller blade (TKE) — 20º inclined propeller blade (velocity vectors)

30º inclined propeller blade (TKE) — 30º inclined propeller blade (velocity vectors)

40º inclined propeller blade (TKE)

40º inclined propeller blade (velocity vectors)

50º inclined propeller blade (TKE)

50º inclined propeller blade (velocity vectors)

60º inclined propeller blade (TKE)
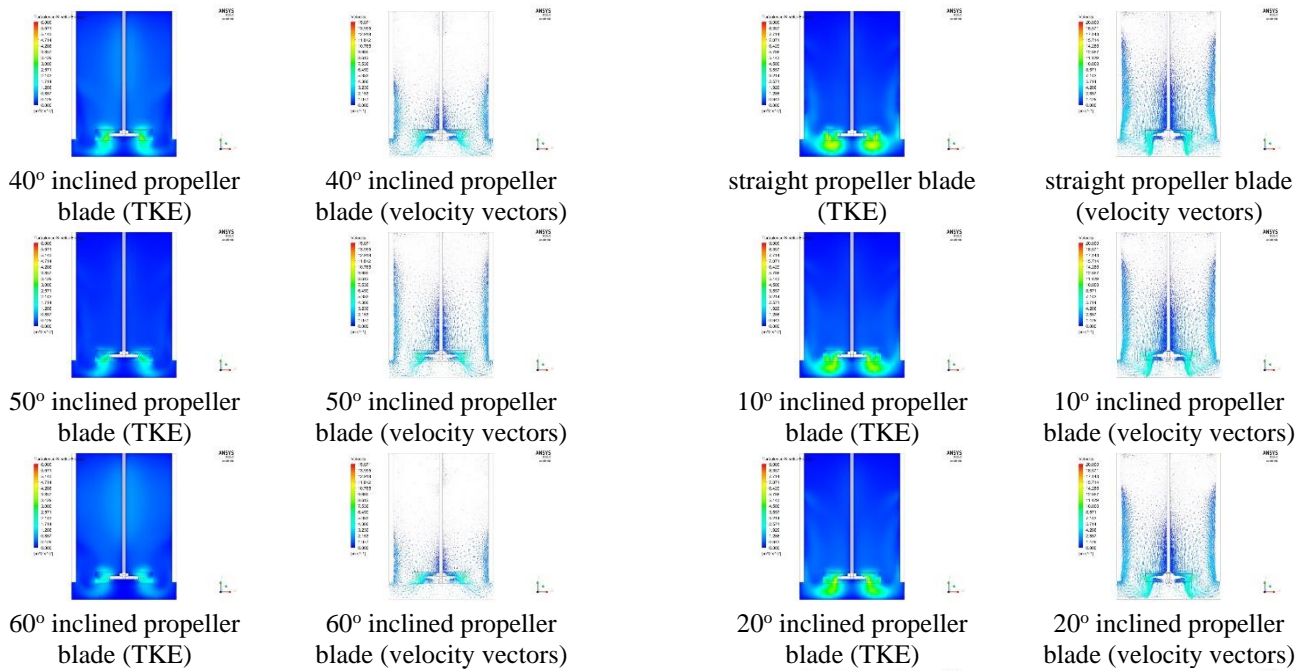
60º inclined propeller blade (velocity vectors)

Figure 6 Model blades at 750 rpm (a) turbulence kinetic energy distribution (b) velocity vectors

Turbulence kinetic energy distributions and velocity vectors obtained for the propellers rotated at 1000 rpm are given in Figure 7 for straight blade, 10° inclined blade, 20° inclined blade, 30° inclined blade, 40° inclined blade, 50° inclined blade and 60° inclined blade, respectively. When these figures are examined, it is seen that turbulence kinetic energy values are high at the blade tips, as in the visuals examined in 600 and 750 rpm. According to the data obtained, it is seen that the maximum turbulence kinetic energy reaches 9000 m2/s2 at 1000 rpm. Looking at the velocity vectors, it was observed that the maximum velocity increased to 20000 m/s. It is more possible to say that the mixture is better with the increase in impeller speed by looking at the values of turbulence kinetic energy and flow velocities obtained. As with other impeller speed, turbulence kinetic energy is observed to be highest in 40° and 50° inclined blade while the lowest levels in the straight and 10° inclined blade throughout the tank.

straight propeller blade (TKE)

straight propeller blade (velocity vectors)

10º inclined propeller blade (TKE)

10º inclined propeller blade (velocity vectors)

20º inclined propeller blade (TKE)

20º inclined propeller blade (velocity vectors)

30º inclined propeller blade (TKE)

30º inclined propeller blade (velocity vectors)

40º inclined propeller blade (TKE)

40º inclined propeller blade (velocity vectors)

50º inclined propeller blade (TKE)

50º inclined propeller blade (velocity vectors)

60º inclined propeller blade (TKE)

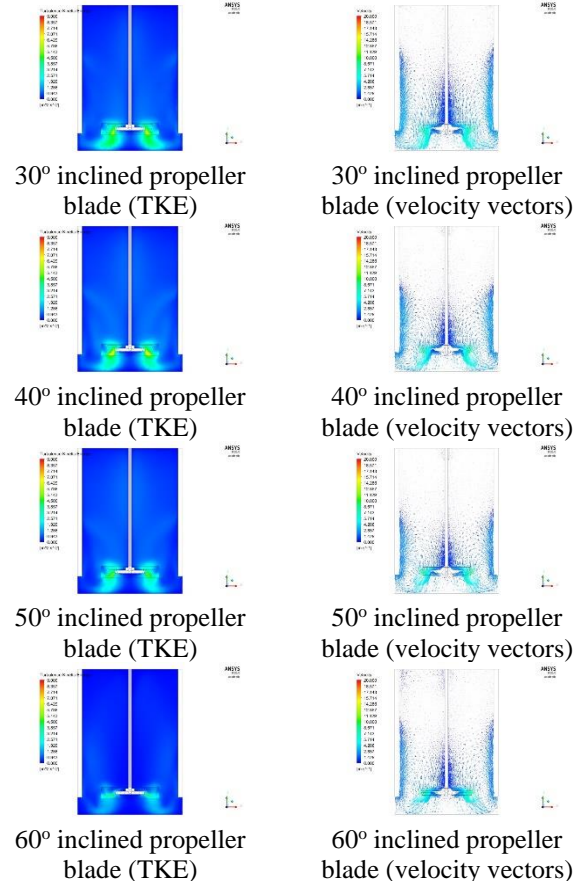60º inclined propeller blade (velocity vectors)

Figure 7 Model blades at 1000 rpm (a) turbulence kinetic energy distribution (b) velocity vectors

The results obtained were compared according to the pressure, turbulence kinetic energy and velocity vectors with respect to the x and y plane. The results for comparison are the data taken from the x and y plane as shown in Figure 8.
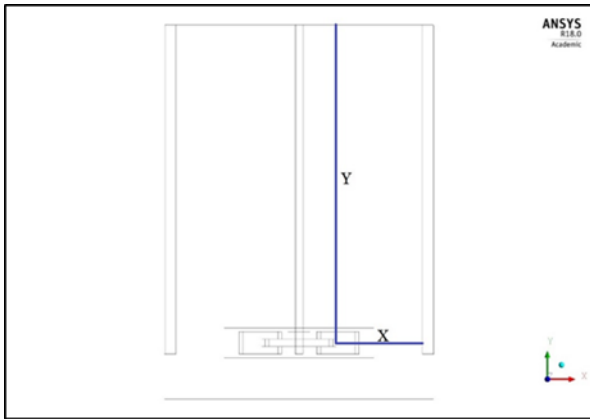
Figure 8 View of the x and y plane evaluated for comparison.

The comparison of the pressure, turbulence kinetic energy and velocity graphs of different propeller models at 600 rpm, respectively, with reference to the x and y plane in Figure 8, is shown in Figure 9. When looked at the x-plane of the pressure graphs in Figure 9a, it was observed that the pressure towards the tank surfaces increased.

Similarly, when the y-plane pressure graphs are examined in Figure 9a, the curves including the pressure created by the straight blade follow a linear path in all blade types. While the pressure of the straight blade towards the upper point of the tank is around 8 kPa, this pressure value decreases as the angle of the other wings increases. The high pressure increases the power consumed for mixing, therefore the highest power consumption requirement was seen in the flat blade here. It is clearly seen from the pressure graphs that at the 60° inclined propeller blade where the pressure is the lowest, lower power consumption will occur.

The change of turbulence kinetic energy along the x and y axis is given in Figure 9b. It is seen that the turbulent kinetic energy decreases from the center to the edges on the x axis. In the y plane, it can be said that the turbulence kinetic energy towards the upper surface of the tank is stable up to a certain level except for the blades inclined 40° and 50°. However, it is possible to say that the 40° and 50° inclined blades generally increase the turbulence kinetic energy in the tank at this point and reach higher levels compared to all other blade models. This increase in kinetic energy shows that turbulence is greater throughout the tank, and therefore blades with 40° and 50° inclinations provide a more homogeneous mixture than straight and other inclined blades. The opposite situation occurs with 10° and 60° inclined blades.

Velocity graphs in x and y axes for 600 rpm are given in Figure 9c. In the x-plane, there was a drop after the effects of the turbulence created behind the blades, and a sudden increase immediately after the fall due to the effect of baffles and reserve flows returning from the tank walls. In the y plane towards the top of the tank; It is seen that the flow velocities in 10 ° inclined and straight blades are higher than the other blades.

The comparison of the pressure, turbulence kinetic energy and velocity graphs of different propeller models at 750 rpm, respectively, with reference to the x and y plane in Figure 8, is shown in Figure 10. The graphics are like at 600 rpm, but the values have increased.

The comparison of the pressure, turbulence kinetic energy and velocity graphs of different propeller models at 1000 rpm, respectively, with reference to the x and y plane in Figure 8, is shown in Figure 11. The graphics are like at 600 rpm and 750 rpm, but the values have increased.
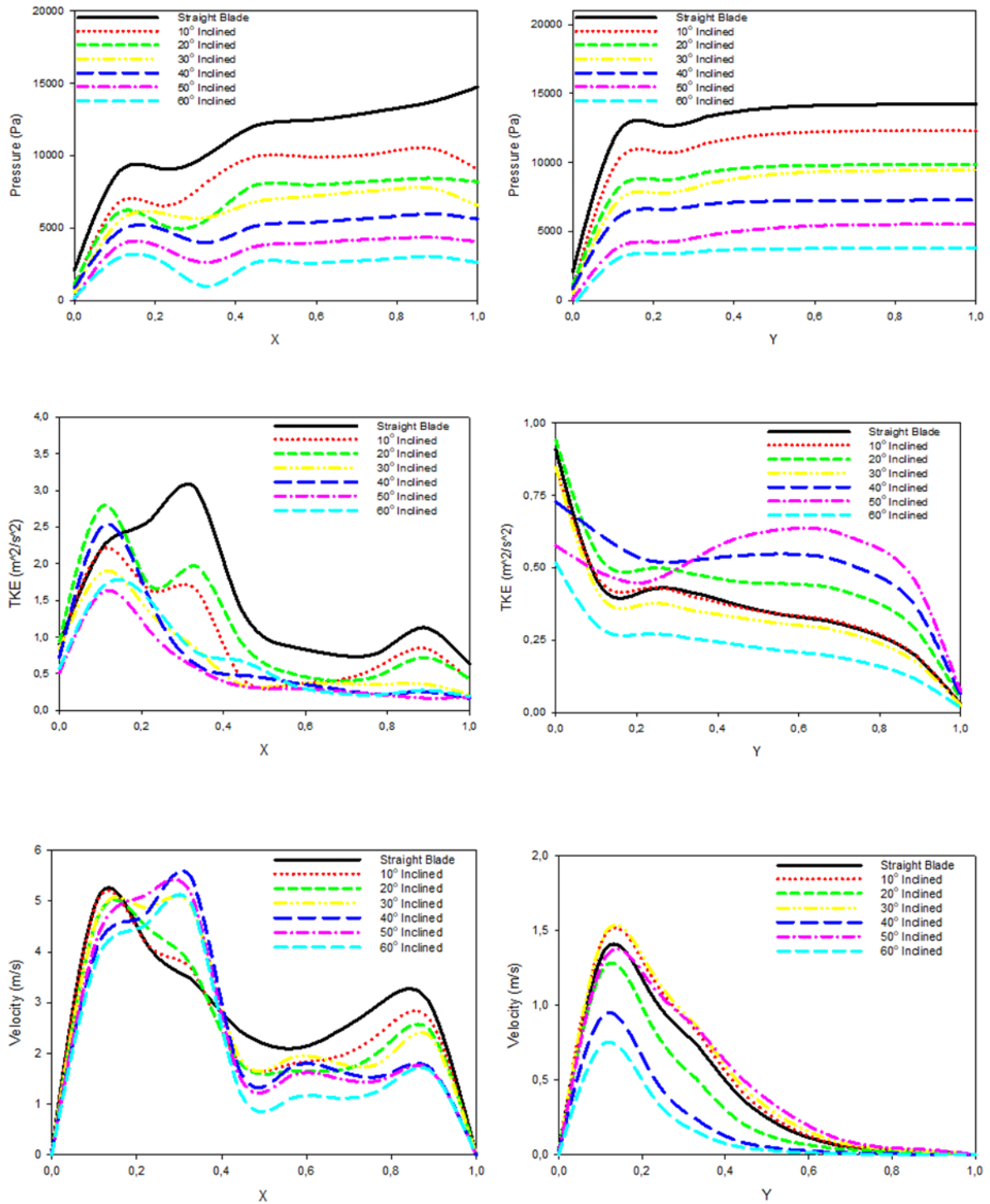
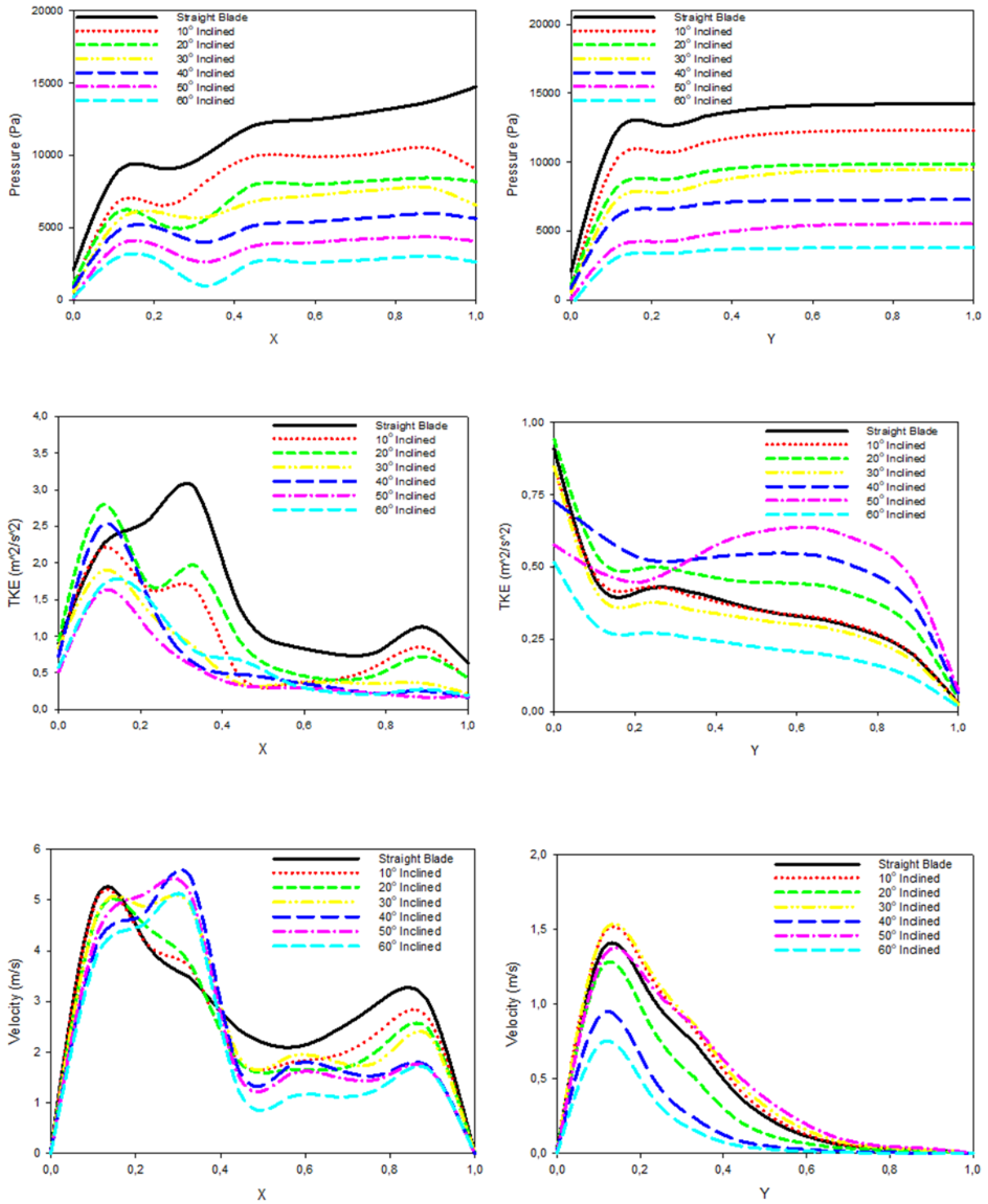Figure 9 Comparison of a) pressure b) TKE c) velocity graphs in the x and y plane at 600 rpm

Figure 10 Comparison of a) pressure b) TKE c) velocity graphs in the x and y plane at 750 rpm
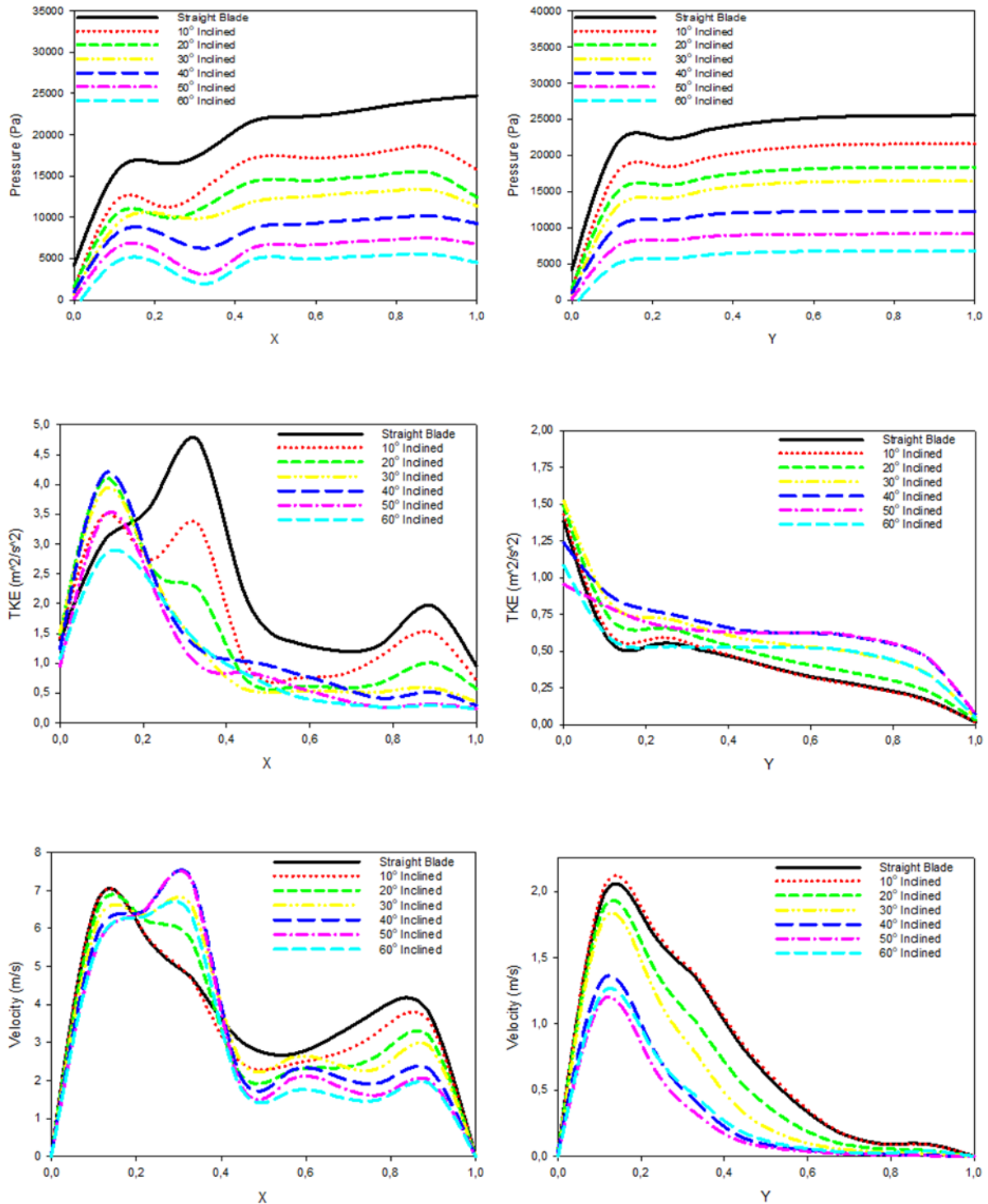
Figure 11 Comparison of a) pressure b) TKE c) velocity graphs in the x and y plane at 1000 rpm

6. CONCLUSİON

In this study, propeller blade types with straight, 10° inclined, 20° inclined, 30° inclined, 40° inclined, 50° inclined and 60° inclined were analyzed numerically.

As a result of the investigation of all the case, it was concluded that the increase in the impeller rotation speed increased the power consumption according to the pressure graphs, but on the other hand, it increased the homogeneity according to the turbulence kinetic energy values. It can be the most accurate result to decide by looking at the material to be used, the power requirement and

the place in the application for the selection of the most suitable rotation speeds.

All of the results showed that increasing the angle of inclination reduced power consumption. The power consumption required by the blades can be listed as high to low straight, 10° inclined, 20° inclined, 30° inclined, 40° inclined, 50° inclined and 60° inclined blades. However, the most effective blade profiles in order to ensure mixture homogeneity have come to the fore as 40° and 50° inclined blades with higher turbulence kinetic energy.

The comparison was made by considering all blade structures and all rotation speeds, the highest turbulence kinetic energy change was seen on the blade 40° inclined in the x and y axis. Although it is concluded that the lowest pressure and therefore the least power consumption are in the blade inclined at 60°, it has been revealed that the turbulent kinetic energy changes cannot provide a homogeneous mixture. However, by comparing the pressure changes, kinetic energy changes and flow rates together, it was concluded that the ideal model was the propeller blade 40° and 50° inclined.

Nomenclature (Word Style TS Strong)

b   Baffle width (m)

D   Impeller diameter (m)

H   Impeller distance from bottom of vessel (m)

g   Acceleration due to gravity (m/s-2)

H   Total liquid depth (m)

k   Turbulent kinetic energy (m2/s-2)

L   Length of blades on impeller (m)

m   Rotating domain height (m)

M   Rotating domain diameter (m)

n   Impeller speed (s-1)

p   Pressure (N.m-2)

s   Clearance of baffle from wall (m)

T   Inside diameter of stirred tank (m)

u   Flow velocity in rotating frame (m/s-1)

v   Flow velocity (m/s-1)

W   Width of blades on impeller (m)

x, y, z Cartesian coordinates

Greek Symbols

μ   Dynamic viscosity (m2/s-1)

ω   Angular velocity (rad/s-1)

Declaration of Competıng Interests

The authors declare no competing financial interests.

REFERENCES

[1]   J. Scully and P. Frawley, "Computational Fluid Dynamics Analysis of the Suspension of Nonspherical Particles in a Stirred Tank," Ind. Eng. Chem. Res., vol. 50, pp. 2331–2342, 2011.

[2]   F. Laurenzi, M. Coroneo, G. Montante, A. Paglianti, and F. Magelli, "Experimental and computational analysis of immiscible liquid – liquid dispersions in stirred vessels," Chem. Eng. Res. Des., vol. 7, no. October 2008, pp. 507–514, 2009.

[3]   E. S. Szalai, P. Arratia, K. Johnson, and F. J. Muzzio, "Mixing analysis in a tank stirred with Ekato Intermig J impellers," Chem. Eng. Sci., vol. 59, pp. 3793–3805, 2004.

[4]   C. P. K. Dagadu, Z. Stegowski, B. J. A. Y. Sogbey, and S. Y. Adzaklo, "Mixing Analysis in a Stirred Tank Using Computational Fluid Dynamics," J. Appl.

Math. Phys., vol. 3, no. June, pp. 637–642, 2015.

[5]   V. I. Bykov and S. B. Tsybenova, "Parametric Analysis of the Continuous Stirred Tank Reactor Model," Theor. Found. Chem. Eng., vol. 37, no. 1, pp. 59–69, 2003.

[6]   S. K. Naeeni and L. Pakzad, "Chemical Engineering Research and Design Experimental and numerical investigation on mixing of dilute oil in water dispersions in a stirred tank," Chem. Eng. Res. Des., vol. 147, pp. 493–509, 2019.

[7]   S. Hosseini, D. Patel, F. Ein-mozaffari, and M. Mehrvar, "Study of Solid - Liquid Mixing in Agitated Tanks through Computational Fluid Dynamics Modeling," Ind. Eng. Chem. Res., vol. 49, pp. 4426–4435, 2010.

[8]   J. Aubin, D. F. Fletcher, and C. Xuereb, "Modeling turbulent flow in stirred tanks with CFD : the influence of the modeling approach , turbulence model and numerical scheme," Exp. Therm. Fluid Sci., vol. 28, no. 2004, pp. 431–445, 2006.

[9]   C. A. Coulaloglou and T. L, L, "Description Of Interaction Processes In Agitated Liquid-Liquid Dispersions," Chem. Eng. Sci., vol. 32, pp. 1289–1297, 1977.

[10] S. K. Naeeni and L. Pakzad, "Droplet size distribution and mixing hydrodynamics in a liquid – liquid stirred tank by CFD modeling," Int. J. Multiph. Flow, vol. 120, 2019.

[11] A. Kazemzadeh, F. Ein-mozaffari, and A. Lohi, "Particuology Effect of impeller type on mixing of highly concentrated slurries of large particles," Particuology, vol. 50, pp. 88–99, 2020.

[12] H. Ameur, Y. Kamla, and D. Sahel, "Data on the agitation of a viscous Newtonian fl uid by radial impellers in a cylindrical tank," Data Br., vol. 15, pp. 752–756, 2017.

[13] D. Gu, Z. Liu, Z. Xie, J. Li, C. Tao, and Y. Wang, "Numerical simulation of solid-liquid suspension in a stirred tank with a dual punched rigid-flexible impeller," Adv. Powder Technol., vol. 28, no. 10, pp. 2723–2734, 2017.

[14] I. González-neria et al., "PIV and dynamic LES of the turbulent stream and mixing induced by a V- grooved blade axial agitator," Chem. Eng. J., vol. 374, no. June, pp. 1138–1152, 2019.

[15] D. Wadnerkar, R. P. Utikar, M. O. Tade, and V. K. Pareek, "CFD simulation of solid – liquid stirred tanks," Adv. Powder Technol., vol. 23, pp. 445–453, 2012.

[16] N. Qi, H. Zhang, K. Zhang, G. Xu, and Y. Yang, "CFD simulation of particle suspension in a stirred tank," Particuology, vol. 11, no. 3, pp. 317–326, 2013.

[17] R. Alcamo, G. Micale, F. Grisafi, A. Brucato, and M. Ciofalo, "Large-eddy simulation of turbulent flow in an unbaffled stirred tank driven by a Rushton turbine," Chem. Eng. Sci., vol. 60, pp. 2303–2316, 2005.

[18] C. J. Ian Torotwa, "A Study of the Mixing Performance of Different Impeller Designs in Stirred Vessels Using Computational Fluid Dynamics," Designs, vol. 2, no. 10, 2018.

[19] Fluent Inc. Lebanon, FLUENT User's Guide. Netherland, 2003.

[20] X. Duan, X. Feng, C. Peng, C. Yang, and Z. Mao, "Numerical simulation of micro-mixing in gas – liquid and solid – liquid stirred tanks with the coupled CFD-E-model," Chinese J. Chem. Eng., vol. 28, no. 9, pp. 2235–2247, 2020.